5

Corrosion processes and the use of corrosion inhibitors in managing corrosion in underground pipelines

V. S. SASTRI, Sai Ram Consultant, Canada

DOI: 10.1533/9780857099266.1.127

Abstract: This chapter reviews the sources of corrosion in underground pipelines carrying oil and gas, such as hydrogen sulfide and carbon dioxide. It also discusses and compares corrosion monitoring techniques, such as linear polarization resistance (LPR), electrochemical impedance spectroscopy (EIS), electrochemical noise (EN) techniques, and the use of sensor probes.

Key words: corrosion, gas pipelines, oil pipelines, corrosion monitoring, linear polarization resistance (LPR), electrochemical impedance spectroscopy (EIS), electrochemical noise (EN).

5.1 Introduction

The petroleum industry consumes a large amount of material. About 8% of the world's production of metals is used in oil production, transport, and processing. The material consumption in the petroleum industry amounts to about 32 kg of metal installed in processing equipment for every ton of processed oil. The enormous quantities of steel and other metals used in the petroleum industry are prone to corrosion to a more marked degree than in other industrial environments. The severity of the problem is such that about 1 kg of steel and other alloys per ton of oil processed is destroyed due to corrosion. Thus, it is clear that corrosion losses in the petroleum industry are considerable, and it is necessary to adopt corrosion mitigation strategies such as the use of corrosion inhibitors and selection of more resistant materials. The costs of processing one cubic meter of processed oil in 1960 are shown in Table 5.1.

Corrosion losses in the petroleum industry amounted to 11 cents per barrel of processed oil, and the losses during distillation were about 65% of the total losses. The corrosion losses of 16 cents per barrel of processed oil and a total cost of corrosion of 450 million dollars in the USA in the oil industry in 1966 have been quoted in the literature.[1] Although these data are old, they stand the test of time with respect to proportional costs.

© 2014 Woodhead Publishing Limited

Table 5.1 The costs of processing one cubic meter of processed oil in 1960

Total expense at the building phase	18.6%
Maintenance and repairs including inhibition costs	61.9 %
Losses connected with unmanufactured products	16.0%
Additional equipment costs	2.3%
Other miscellaneous expenses	1.2%

The data on economics of corrosion in the oil industry, although many decades old, illustrate the need for urgent attention toward efforts to mitigate corrosion in the oil industry. One of the most prudent and economic methods of combating corrosion in the oil industry is the use of corrosion inhibitors. According to the literature, the cheapest method of combating corrosion in oil pipelines is the use of corrosion inhibitors. According to Bregman, the ratio of preventable losses to inhibitor costs ranges from 4:1 to 7:1. Other methods of corrosion control, such as the use of more corrosion-resistant alloys or protective coatings, are more expensive than the use of corrosion inhibitors. Another attractive feature is that corrosion inhibitors can be applied for the protection of partially corroded equipment.

5.2 Sources of corrosion in oil and gas production

The main corrosive media and processes in the oil industry are:

- hydrochloric acid and its aqueous solutions
- hydrogen sulfide
- corrosion of steel at hydrocarbon–electrolyte interfaces
- corrosion of steel in emulsified two-phase environments
- oxygen
- naphthenic acids
- carbon dioxide.

5.2.1 The role of hydrogen sulfide in corrosion

Carbon dioxide and/or hydrogen sulfide are known to be very corrosive species in the corrosion of metals or alloys used in pipes and other tubular goods and equipment. Hydrogen sulfide is particularly harmful since it can cause sulfide stress corrosion cracking (SSCC) failure in the pipe. When high strength steel having a Rockwell hardness, R_c, in excess of 22–25 is used, sulfide cracking may occur in the form of spontaneous brittle fracture,

probably resulting from hydrogen embrittlement. Carbon steels of lower hardness are not as susceptible to sulfide cracking, but are sensitive to pitting corrosion and general corrosion in the presence of chloride. Extensive literature on the effect of hydrogen sulfide on the failure of equipment in the oil and gas industry is available.[2] Corrosion problems encountered in the oil and gas industry as related to the use of inhibitors and the mechanism of corrosion due to hydrogen sulfide are discussed in the literature.[3–15]

Hydrogen sulfide is corrosive only when it is dissolved in water. The solubility of hydrogen sulfide in water is relatively high compared to carbon dioxide and oxygen, which are the main corrosive gases present in oil and gas production systems. The acidity due to the presence of H_2S is further enhanced by carbon dioxide, which is usually present in the system. The overall process is represented by the obviously oversimplified equation:

$$Fe + H_2S \xrightarrow{H_2O} FeS + H_2S \qquad [5.1]$$

It has been shown that the corrosive effect is weak when the water content of the production fluid is low. The corrosion products are formed over the metal surface as a black powder, or as a more or less compact layer of a deposit/scale, which can reduce the rate of corrosion, with the extent of the effect dependent on the stability, crystallinity and permeability of hydrogen and the rate of formation of the corrosion product sulfide layer. The protective properties of the sulfide layers increase with increasing temperature, and the susceptibility of the underlying steel to SSCC decreases. The SSCC has been found to decrease at 65°C for high strength steel. The protective layers of troilite (Fe_7S_8), pyrrhotite ($Fe_{1-x}S$), kansite (Fe_9S_8) and mackinawite ($Fe_{1+x}S$) may be formed depending on pH, H_2S concentration, and other species such as chloride and CO_2. The nearly perfect crystal lattices of pyrite and troilite give better corrosion protection than the less perfect kansite.

It is useful to note that the sulfide layer should influence the kinetics of the corrosion processes. In the absence of oxygen, the parabolic character of iron sulfide formation was shown, i.e. a linear relation of the corrosion rate with the square root of time, indicating that the corrosion rate decreases as the iron sulfide film thickness increases.

A detailed review of the current theories of the basic steps involved in the corrosion mechanism initiated by hydrogen sulfide may be found in the literature.[16] The most probable mechanism suggested involves interaction of bisulfide (HS^-) ions on the surface of the metal with H_3O^+ ions from the electrolyte to form a catalytic complex, Fe $(H—S—H)_{ads}$. The protons of this surface complex give rise to hydrogen atoms due to cathodic polarization.

The hydrogen atoms may also recombine to form molecular hydrogen or diffuse into the metal:

$$Fe + HS^{-} \rightleftharpoons Fe\left(HS^{-}\right)_{ads} \quad [5.2]$$

$$Fe(HS^{-})_{ads} + H_3O^{+} \rightarrow Fe\left(H{-}S{-}H\right)_{ads} + H_2O \quad [5.3]$$

$$Fe\left(H{-}S{-}H\right)_{ads} + e^{-} \rightarrow + Fe(HS^{-}) + H_{ads} \quad [5.4]$$

The step involving the interaction of Fe (H–S–H) with an electron is thought to be the rate-determining factor of the cathodic reaction. The explanation has been given for the anodic reaction involving an adsorption complex:[17]

$$Fe + H_2S + H_2O = Fe(HS^{-})_{ads} + H_3O^{+} \quad [5.5]$$

$$Fe(HS^{-})_{ads} \rightarrow (FeHS)^{+} + 2e^{-} \quad [5.6]$$

$$Fe(HS)^{+} + H_3O^{+} \rightarrow Fe^{2+} + (H_2S) + H_2O \quad [5.7]$$

An intermediate complex such as Fe/H_2S ad. that generates H_2S has been proposed:[18]

$$Fe(H_2S) \rightarrow Fe\left(H_2S\right)_{ads} \quad [5.8]$$

$$Fe(H_2S)_{ads} \rightarrow Fe\left(H_2S\right) + 2e^{-} \quad [5.9]$$

$$(Fe{-}H_2S)^{2+} \rightarrow Fe^{2+} + (H_2S) \quad [5.10]$$

Another hypothesis is based on H_2S as the stable species in an acidic solution and not HS^{-} and, as a result, $Fe{-}H_2S$ will be the transient complex in the anodic reaction.[19] In the cathodic reaction, which is also accelerated in H_2S, there is a diversity of opinion, especially about the presence of HS^{-} in acid media. A suggestion has been made that the discharge of hydrogen occurs by the formation of protonated H_2S, which is more readily formed than H_3O^{+}:

$$(H_2S)_{ad} + H_3O^+ \rightarrow HH_2S^+_{ads} + H_2O \quad [5.11]$$

$$(HH_2S)^+_{ad} + e^- + M \rightarrow H - M - (H_2S)_{ad} \quad [5.12]$$

$$H_3O^+ + e^- + M \rightarrow H - M + H_2O \quad [5.13]$$

The cathodic reaction has been studied in detail by many authors.[20–22]

There is relatively little information in the literature on the localized corrosion in sour gas environments. Localized corrosion can occur by the formation of iron sulfide spots on the metal surface, which can lead to the formation of iron–iron sulfide electrochemical local cells. According to one school of thought, the composition and nature of corrosion products of the Fe_xS_y when acting as the cathode would be more important in determining a corrosion mechanism than the influence of dissolved hydrogen sulfide. The iron sulfide on the surface, primarily pyrrhotite, is an effective cathode. The anodic reaction under the sulfide layer will depend on the presence of aqueous solution at the FeS interface. Traces of polysulfide may also be formed by the reaction of H_2S with sulfur or other oxidizing agents present in the system, which can lead to the occurrence and development of localized corrosion. The nature of polysulfide species in acid media is not yet completely understood. Potentiometric studies have shown that small concentrations of H_2S react with oxidizing agents, resulting in the formation of small amounts of H_2S_2 and colloidal sulfur at temperatures up to 90°C, which leads to localized corrosion.[23]

5.2.2 The role of chloride in corrosion

The other important corrosive species is chloride, which is present in the mineralized water present at the well bottom. Corrosion due to chloride is more severe at high temperatures. Failures due to chloride can be due to intergranular corrosion and chloride stress corrosion cracking (CSCC). Both intergranular corrosion and CSCC involve anodic dissolution as a step for crack propagation. CSCC failures can occur in many materials, ranging from low alloy steels to super alloys. CSCC failures can be dangerous for parts of equipment exposed to aerated environments.

The simultaneous presence of sulfide and chloride corrosion has been observed in de[illegible]our gas production.[24,25] The sour gas is mainly methane under high pressure without liquid hydrocarbons present. The corrosion mechanism advanced consists of the formation of 'scabs' of iron sulfide products involvi[illegible]oth H_2S and chloride ions. The thin liquid film on the

metal surface in an acid gas environment will contain hydrochloric acid, which reacts with hydrogen sulfide to form iron chloride. The hydrogen sulfide in the gas reacts with iron chloride to form scab-like iron sulfide and regenerates the chloride ion, which reacts with more iron. This sequence of reactions results in high corrosion rates.

$$Fe^{o} + HCl \rightarrow FeCl_2 \quad [5.14]$$

$$FeCl_2 + H_2S \rightarrow FeS + 2HCl \quad [5.15]$$

5.2.3 The role of carbon dioxide in corrosion

Carbon dioxide is commonly produced along with gas and oil. Carbon dioxide dissolves in water to form carbonic acid, resulting in a decrease in pH. The corrosion caused by CO_2 is termed as 'sweet'. The corrosion due to CO_2 can also arise due to the injection as a method for enhanced oil recovery, which can cause downhole corrosion, and corrosion of surface equipment. A characteristic feature of CO_2-induced corrosion is pitting, which is manifested in the form of deep, sharp-edged pits. Carbon dioxide may also cause general corrosion in heat-affected zones such as welds. In deep wells, carbon dioxide forms a carbonate scale with corrosion in turbulent areas. The partial pressure of CO_2 in production fluid is cited as a controlling factor governing the corrosive attack. The following relationship has been put forward.[26]

- A partial pressure of CO_2 above 30 psi usually indicates corrosion.
- At partial pressures of 3–30 psi, corrosion may occur.
- At partial pressures below 3 psi, corrosion is generally negligible.

This rule of thumb is applicable to gas wells only. A more commonly used relationship to predict the corrosivity of acidified CO_2 brines is based on the equation due to deWaard and Williams.[27] Assuming the reduction of carbonic acid as a rate-determining step, the corrosion rate is given by the equation:

$$\text{Log. } c.r. = 0.67\left(\log P_{CO_2}\right) + c \quad [5.16]$$

where $c.r.$ is the corrosion rate, P_{CO_2} is the partial pressure of CO_2, and c is a constant.

The detailed mechanism of CO_2 corrosion in oil and gas production and advances in CO_2 have been documented in the literature.[28] The mechanism involved in CO_2-induced corrosion has been discussed in the literature. In the presence of oxygen, it is essentially the same as in oxygen alone at the same pH. In the absence of oxygen, the mechanism is as shown below in Fig. 5.1. The cathodic reaction is:

$$2CO_2 + 2H_2O \rightleftharpoons 2H_2CO_3 \xrightarrow[+2e^-]{2H^+\ 2HCO_3^- + 2e} H_2 + 2HCO_3^- \qquad [5.17]$$

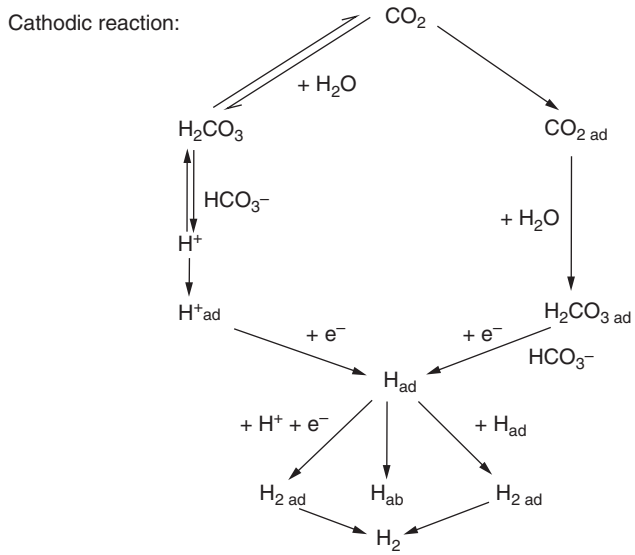

$$2CO_2 + 2H_2O \rightleftharpoons 2H_2CO_3 \xrightarrow[+2e^-]{2H^+ + 2HCO_3^- + 2e^-} H_2 + 2HCO_3^-$$

Anodic reaction:

$$Fe + H_2O \rightleftharpoons FeOH_{ad} + H^+ + e^-$$

$$FeOH_{ad} \rightarrow FeOH^+ + e^-$$

$$FeOH^+ + H^+ \rightleftharpoons Fe^2 + H_2O$$

$$Fe \rightarrow Fe^{2+} + 2e^-$$

Total reaction:

$$Fe + 2CO_2 + 2H_2O \rightarrow Fe + 2H_2CO_3 \rightarrow Fe^2 + H_2 + 2HCO_3^-$$

5.1 'Sweet corrosion' (in oxygen-free CO_2 solution).

The anodic reaction is:

$$Fe + H_2O \rightleftharpoons FeOH_{ad} + H^+ + e^- \quad [5.18]$$

$$FeOH_{ad} \rightarrow FeOH^+ + e^- \quad [5.19]$$

$$Fe(OH)^+ + H^+ \rightleftharpoons Fe^{2+} + H_2O \quad [5.20]$$

$$Fe^o \rightarrow Fe^{2+} + 2e^- \quad [5.21]$$

The total reaction is:

$$Fe + 2CO_2 + 2H_2O \rightarrow Fe + 2H_2CO_3 \rightarrow Fe^{2+} + H_2 + 2HCO_3^- \quad [5.22]$$

The ideas on which some of the conclusions and statements, based on factors such as pH, CO_2 partial pressure, temperature, water and gas production rate, have been criticized,[29] since it was considered that these represent an overall or average assessment of downhole corrosion processes and fail to account for localized corrosion, which is the cause of the failure. By measurements in 60 gas wells with large variations in production characteristics,[30] tentative correlations between general and localized corrosion rates have been made.

Two different mechanisms dependent on temperature have been identified. Below 60°C, the corrosion rate is controlled by the rate of diffusion of CO_2 to the metal surface or the rate of hydrolysis of CO_2 to form carbonic acid. Above 60°C, iron carbonate, $FeCO_3$, is formed on the metal surface, and the rates of all corrosion processes are controlled by the transfer across the iron carbonate layer. It is surmised that localized corrosion arises when the transition from the carbonic acid formation reaction to the formation of ferrous carbonate on the metal surface[31] takes place.

In the general case, the corrosion rate depends upon the permeability of the scale as well as a combination of intrinsic scale dissolution and flow rate. The rate of dissolution of iron carbonate has been found to be relatively slow, and hence the flow regime becomes the predominant factor in determining the corrosion rate in gas wells. The kinetics of corrosion reactions in the presence of an interlayer of corrosion products between the metal and corrosion media have been studied extensively.[32]

The variety of corrosion products formed in CO_2 saturated systems are: iron carbonate scale or mixed iron hydroxy-carbonate, iron-calcium carbonate, are formed, which decrease the corrosion rate.[33,34] The impact of

corrosion products on the flow dependence has been under dispute since this effect had been observed by some authors,[35,36] while this was not observed by others,[37–39] which may be due to the different corrosion mechanism in operation at low temperatures and low CO_2 partial pressures and the absence of corrosion products opposed to higher temperatures and pressures and the presence of corrosion product layers. The corrosion rates of carbon steel and some high alloy steels in the presence of iron carbonate ($FeCO_3$), as a function of temperature, partial pressure of CO_2, have been determined.[40,41]

Corrosion in oil and gas production also results in corrosion-erosion or flow-induced localized corrosion in CO_2 containing brines, related with the fact that the actual production at greater depths, at higher temperatures and pressures, and the use of smaller bore tubing results in higher velocities of the production stream. The system experiences a radical change with the introduction of a small amount of H_2S. Iron sulfide is formed as a thermodynamically stable product instead of $FeCO_3$, and magnetite may be formed at high temperatures even in the presence of high partial pressures of CO_2.[42] The low solubility of magnetite and electron conductivity compared with carbonate scale leads to pitting corrosion.[42] Magnetite may form up to 121°C, and a mixture of siderite and iron sulfide have been detected[43] at a partial pressure ratio of $CO_2/H_2S = 500$. The corrosion rate due to CO_2 may also be reduced in systems when a turbulent flow disperses the water in the hydrocarbon phase, preventing it from reaching the steel surface.[44]

5.2.4 The role of oxygen in corrosion

The role of oxygen as a corrosive agent in secondary recovery by water flooding is important. Injection water usually contains dissolved salts and a small amount of oxygen, which can cause extensive corrosion due to oxygen differential concentration cells. Corrosion due to dissolved oxygen results in pits in the drill pipe, which under stress initiate an easily propagated fatigue crack leading to failure. Oxygen causes extensive damage to water injection equipment, such as pumps, piping, water storage tanks, and injection well tubing, and the corrosion products may plug the formation. Although the role of oxygen is not well understood, the dissolved oxygen is removed mechanically by vacuum deaeration or gas stripping. Vacuum deaeration or gas stripping is not very efficient and hence an oxygen scavenger such as sodium sulfite, together with cobalt nitrate on hydrazine, is used in the removal of oxygen from the system. Hydrazine is toxic and its performance as an oxygen scavenger is not very satisfactory in comparison with sulfite or bisulfite mixed with cobalt nitrate. Oxygen-induced corrosion can be minimized by the use of inhibitors.

5.2.5 The role of bacteria in corrosion

The role of bacterial corrosion due to microorganism activity can be a significant problem, particularly in enhanced recovery processes such as water flooding. Several forms of bacteria contribute to corrosion and the most common ones are sulfate-reducing and iron bacteria. The bacteria may cause corrosion of piping, plugging of the injection or disposal wells, and souring of the fluids and reservoir. Microbiologically influenced corrosion (MIC) had been extensively studied from the industrial practice point of view, in order to arrive at cost-effective solutions in monitoring large water injection systems.[45–48] In order to avoid expensive and inefficient treatments for microbiological corrosion that are sometimes applied in industrial practice, one must direct efforts toward predicting microbiologically induced corrosion (MIC), development of efficient biocides, thorough understanding of MIC mechanisms, and better control of the eventual conversion of sweet to sour production that can be caused by sulfate-reducing bacteria. The current trends in the investigation of MIC have been discussed from the point of view of a practicing corrosion engineer facing complex corrosion control in the oilfield.[45]

When seawater is used in injection systems, the oxygen present can initiate severe damage of pumps, vessels, injection lines, and downhole injection well equipment by pitting, and can also promote growth of aerobic bacteria, leading to the formation of a biofilm on the metal surface under which sulfate-reducing anaerobic bacteria could be formed.[47] The sulfate-reducing bacteria, produced by algae or by the dense gelatinous deposits produced by iron bacteria, can be enhanced by the presence of calcium carbonate scale.[8] Biocidal treatment is equally important as that of corrosion, and can have important implications on the choice of chemical treatment of the injection water with respect to chemical compatibility.

5.3 Techniques used in monitoring corrosion inhibitors in oil and gas pipelines

Oil and gas pipeline flows are multiphase in nature, consisting of oil, aqueous (brine water), and gas phases. One of the main risks of operation of the oil pipelines is internal corrosion in the form of pitting corrosion. By ascertaining the conditions leading to corrosion, suitable strategies can be adopted to combat corrosion by, for instance, addition of suitable corrosion inhibitors, at the requisite concentrations, and/or adjusting fluid flow rate. Thus, monitoring corrosion in underground or above ground oil and gas pipelines is a crucial step in the integrity management process. In an ideal case, a monitoring technique should provide data on the effect of inhibitors on both general and pitting corrosion.

In practice, a single monitoring technique is incapable of providing data on both general and pitting corrosion. Hence, a suite of techniques are used to obtain reliable data on both general and localized corrosion. When different techniques are used, the benefits and limitations should be clearly understood, especially when the corrosion rates obtained by different methods are used to develop integrity management programs. Many factors are involved in obtaining corrosion rates from the measured parameters. The process of extraction of corrosion rates from the measured data can sometimes be complex depending on whether the data are averaged (weight loss), instantaneous (e.g. LPR and electrochemical impedance spectroscopy (EIS)), or continuous monitoring, as for example electrochemical noise (EN) monitoring.

Detailed studies on the reliability of weight loss, linear polarization resistance (LPR), EIS, EN, and externally mounted hydrogen sensor probes for monitoring performance of corrosion inhibitors in operating oil and gas pipelines have been made.[49] The loop that could take the full flow of the pipe was made of carbon steel. The loop shown in Fig. 5.2 had three pipe sections, namely inlet, replaceable, and outlet – each with a length of ~5 ft (1.5 m). The loop was attached to the operating pipeline through valve no. 1. The valve led to a 3 inch (7.62 cm) pipe, which had two ports. At the first port, a two-strip coupon ladder (preinjection) was attached, and the second port was used for injection of the inhibitor. The 3 inch pipe was attached to the inlet section that was 6 inches (15.24 cm) in diameter and

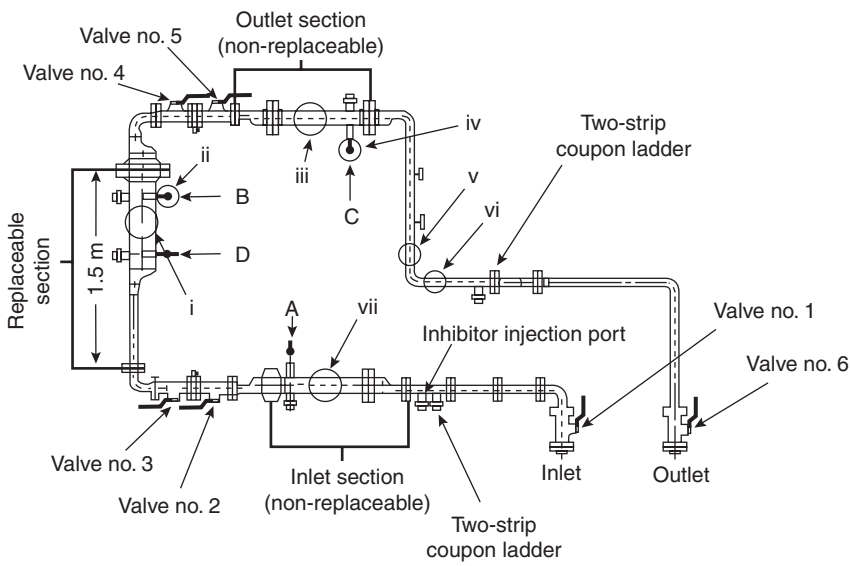

5.2 Schematic diagram of field loop.

37.2 inches (94.5 cm) long. The 6 inch section was off-centered with respect to the 3 inch pipe section in such a way that the expansion from 3 inches to 6 inches was downward. The 6 inch experimental section contained Ladder A (a three-pair, tree-coupon ladder) 32.4 inches (81 cm) from the 3 inch to the 6 inch expansion. At the other end (replaceable section end) of the inlet section, a 6 inch to 3 inch reducer was attached, which, in turn, was attached to two valves, 2 and 3, and finally to a 90° bend. The replaceable section was attached at the opposite end of the bend.

The replaceable section had a 3 inch pipe and a 6 inch or 10 inch pipe, depending on the field section. The 6 inch experimental pipe section was off-centered with respect to the 3 inch pipe section in such a way that the expansion from the 3 inch pipe to the 6 inch pipe was downward (i.e., the expansion was done such that the tops of the two pipes were level and the bottom of the 6 inch pipe was curved up to complete the weld. The 6 inch (or 10 inch) section was attached with two three-pair, tree-coupon ladders (Ladder B and Ladder D). The distance between the 3 inch to 6 inch expansion and Ladder B was the same as that between the 3 inch to 6 inch expansion and Ladder A. Ladder D was placed closer to the 3 inch to 6 inch expansion at 7.2 inches (18 cm). At the other end (outlet section end) of the replaceable section, a 6 inch to 3 inch reducer was attached, which in turn was attached to a 90° bend.

At the opposite end of the 90° bend, two valves (no. 4 and no. 5) were attached. Valve no. 5 was attached to a 3 inch to 6 inch expansion, which in turn was attached to the outlet section. The outlet section had 6 inch and 3 inch pipe sections. The 6 inch experimental section was off-centered with respect to the 3 inch valve section, such that the 3 inch to 6 inch expansion was downward. This section contained Ladder C (a three-pair, tree-coupon ladder) 32.4 inches (81 cm) from the 3 inch to 6 inch expansion, as in the inlet and replaceable sections. The 6 inch section was attached to a 3 inch pipe section. The 3 inch pipe section had a 90° bend, a 60 inch (150 cm) straight section, another 90° bend and another 32 inch (80 cm) straight section that was attached to the operating pipeline through valve no. 6. Just before valve no. 6, a two-strip coupon ladder (post-injection) was inserted in the 3 inch pipe section.

The operating conditions in the three fields are presented in Table 5.2. The field experiments were conducted in three types of fields, namely:

- gassy-oil field,
- oily-gas field,
- oil-transmission field.

For every experiment in every type of field, a new replaceable section (10 inch diameter) was used. The samples (coupons) as well as the replaceable section

Table 5.2 Operating conditions during field experiments

Conditions	Gassy-oil	Oily-gas	Oil-transmission
Gas production rate, m^3/day	17×10^3	122×10^3	This pipe section carries 99.5%
Oil production rate, m^3/day	49	28	oil with less than 0.5% water
Water production rate, m^3/day	170	31	
Gas composition	20% H_2S + 2.5% CO_2, balance hydrocarbon		Less than 0.5% H_2S + 0.5% CO_2
Temperature (°C)	60	55	55
Pressure, psi	250	250	Atmospheric
Replaceable pipe section, in.	6	10	10
Diameter of the operating pipe in the field, in.	6	10	1
Inhibitor, continuous batch	No. 1[a] and No. 3[a] No. 2[b] and No 4[c]	No. 5[d] No. 6[d]	No. 2
Concentration, ppm continuous batch	0, 50, 100, and 200 0 and 2000	0, 100, 250, 500, 1000 0 and 5000	0 and 2000

[a]Water-soluble.
[b]Oil-soluble, water-dispersible.
[c]Oil-soluble.
[d]Compositions not known.

exposed to the oil-transmission field were subjected to prepitting by drilling, punching, chemical, and electrochemical methods.[50,51] The pre-pits in each area were arranged in an arc at angles of 70, 80, 90 and 110°. On the coupon samples, the pre-pits were aligned in a row from top to bottom.

The concentrations or injection levels of inhibitors were adjusted relative to the volume of the production brine water. During batch inhibitor treatment, the pipe loop, along with coupons, was treated with a kerosene solution of the inhibitor. At each inhibitor level, the experiments were done for 15 days in gassy-oil and oily-gas fields, and for 30 days in an oil-transmission field. A new set of coupons was used for every inhibitor concentration used.

All four coupon ladders (A, B, C, and D) were used and, for a particular inhibitor concentration, there were eight – each of top, middle and bottom coupons. Of these eight coupons, four coupons were 'standard coupons' and four were made from pipe material. The chemical analysis of the pipe and standard coupons is given in Table 5.3. The 76 mm × 19 mm × 3 mm coupons

Table 5.3 Chemical composition of pipe and standard coupons

	Compositions (%)		
Element	Standard coupons	Pipe coupons	Difference
C	0.23	0.2	0.03
Si	0.24	0.18	0.06
Mn	0.72	0.63	0.09
Cr	0.08	0.072	0.08
Ni	0.06	0.049	0.01
Mo	<0.03	<0.03	0
Cu	0.17	0.18	0.01
Al	<0.006	<0.006	0
Nb	<0.01	<0.01	0
V	<0.01	<0.01	0
Ti	<0.01	<0.01	0
B	0.004	0.004	0
P	0.01	0.01	0
S	0.02	0.013	0.01
W	–	<0.02	–
Sn	–	0.0081	–
Co	–	0.0045	–
Zr	–	<0.002	–
Pb	–	<0.01	–

were positioned in such a way that the thickness of the coupons was facing the flow.

The two bottom and one of the middle six coupons on each ladder were wired for electrochemical monitoring. The wires were silver soldered onto the coupons. The junctions and electrical wires were covered with chemical-resistant epoxy. The ladder head and controlling instrument cable were connected using a military-standard six-pin receptacle. LPR and electrochemical impedance spectral (EIS) measurements were performed with a potentiostat.

EN was measured with an IL-channel instrument. Four of the twelve channels of the instrument were activated to collect data from the four ladders. The data were automatically logged. The activated channel was allowed to achieve steady state for 10 min, after which 1024 data points at a rate of 2 s per point were collected. The data collection was switched to another channel, and the process was repeated intermittently, and the potentiostat was used to make LPR and electrochemical impedance measurements.

Hydrogen flux through the pipe wall was monitored using pressure-sensitive foils, and their location is shown in Fig. 5.1. The foils were positioned at the bottom, or side, or top of the loop at 6, 9, or 12 o'clock positions respectively. Two foils were attached to the sides of traps. The stainless steel foils (15 cm × 10 cm or 15 cm × 15 cm) were glued to the external surface of the

pipe, creating a hermetic chamber. A 10 foot long capillary tubing welded onto the foil connected the chamber to a manometer. A vacuum of nearly 90 kPa was established, and the hydrogen flux was monitored by the increase in internal pressure (or vacuum loss).

The pipe sections, 6 inch replaceable section (after gassy-oilfield), 10 inch replaceable section (after oily-gas field), and 10 inch replaceable inlet and outlet sections (after oil-transmission field) were cut horizontally into two halves at 3 o'clock and 9 o'clock positions. Each piece was cut further to measure the pit distribution in 6 inch to 3 inch reducer 3 inch pipe, 3 inch to 6 inch expansion, 6 inch pipe, elbow, and trap wall. In each region, the 50 largest pits were measured and the average pit depths and standard deviations were calculated. Similarly, the pit depths in the coupon samples were measured.

5.4 Measuring pitting corrosion rates

The pit distribution in coupons exposed for 15 days without inhibitor, and the replaceable pipe section exposed for 1 year in the gassy-oil field, are shown in Fig. 5.3. In this figure, three types of pits, namely pits at 9, 12, and 3 o'clock positions (top in gas-oil phase), pits at the 6 o'clock position (bottom, in the oil-water phase), and pits at the 6 o'clock position (water phase)

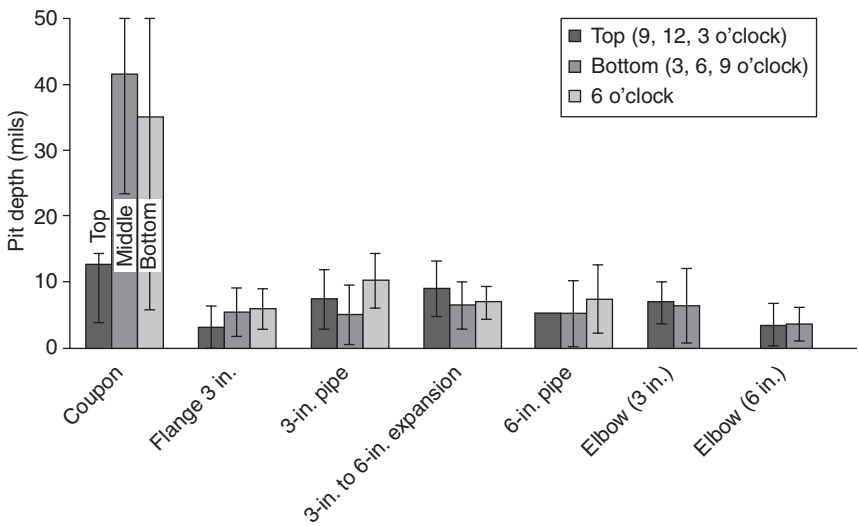

5.3 Comparison of pit depths in the coupons (no inhibitor, 15 days) and in the replaceable pipe section (1 year) exposed in gassy-oil field (refer to Fig. 5.2 for different sections of the pipe).

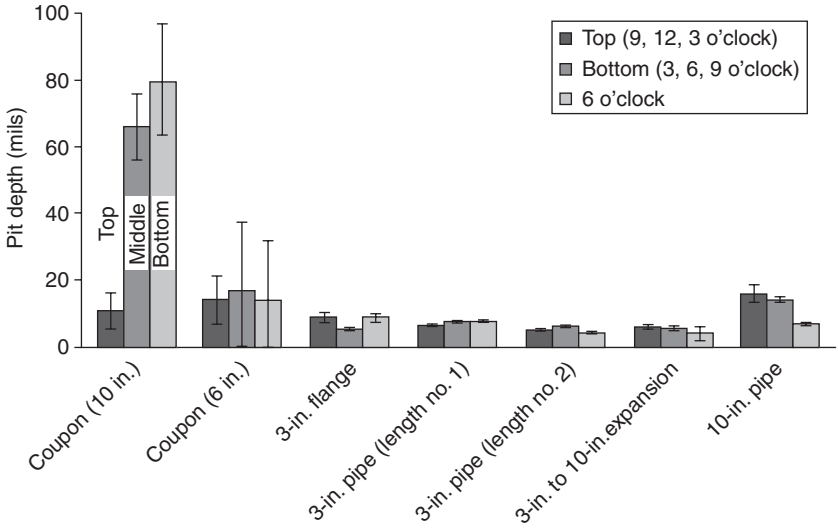

5.4 Comparison of pit depths in the coupons (no inhibitor, 15 days) and in the replaceable pipe section (8 months) exposed in oil-gas field (refer to Fig. 5.2 for different sections of the pipe).

are shown. The pits in coupons exposed for 15 days are nearly four times deeper than those in the pipe exposed for 1 year.

The comparison of pit depths in the coupons and the replaceable section of the pipe exposed to the oil-gas phase are shown in Figs 5.3 and 5.4. The pits in coupons exposed for 15 days are much deeper than the pits in the pipe exposed for 8 months. Out of the four coupon ladders, two were exposed in the 10 inch section (Ladders B and C) and two were exposed in the 6 inch section (Ladders A and D) of the pipe loop.

A comparison of the pit depths in coupons and in the replaceable section of the pipe exposed to an oil-transmission field is depicted in Fig. 5.5. Because of the lower water content of the pipeline, no appreciable growth of the pits was noted, either in coupons or in the pipe except for some pitting in the 10 inch pipe section with particular reference to the region near the expansion from 3 inch to 10 inch pipe.

Pit distribution in the inlet and outlet sections, which are exposed to all three fields and under all inhibitor concentrations, are shown in Fig. 5.6. The pit depths in the inlet and outlet sections of the pipe loop exposed for nearly 2 years are smaller than those of coupons exposed for ~15 days. Figure 5.7 represents the general corrosion rates of standard vs pipe coupons exposed for 15 days. No marked differences were noted between the two sets of coupons, although the standard coupons (Type 1018 mild steel (UNS 10180) were polished successively to 600 grit finish, while pipe sample

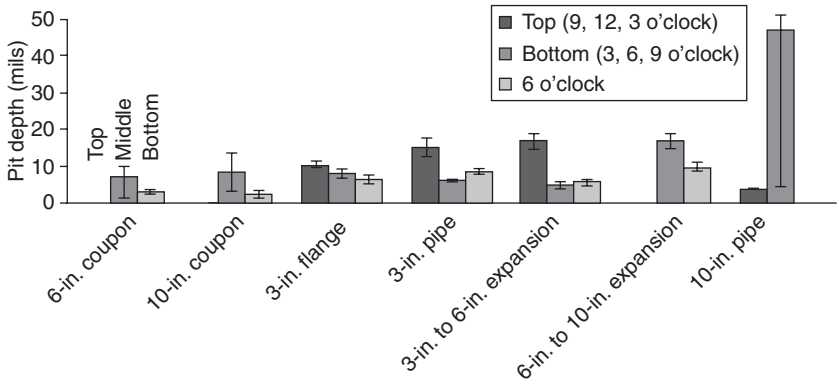

5.5 Comparison of pit depths in the coupons (treated with 5000 ppm of Batch Inhibitor No. 6, 30 days) and in the replaceable pipe section (3 months) exposed in oil-transmission field (refer to Fig. 5.2 for different sections of the pipe).

coupons (ASTM A106Gr.B) were grit blasted better than a white finish. Both the compositions (Table 5.3) and the corrosion rates are similar. It is to be noted that polishing and metallurgical differences have little effect as opposed to the location of the sample. General corrosion rates obtained by various techniques on the same coupon are illustrated in Figs 5.8– 5.10.

The corrosion rates obtained from weight loss and hydrogen foil data are shown in Fig. 5.11. The weight loss and pressure loss data were obtained from coupons exposed to pipeline and the hydrogen foil probes on the external surface of the pipe respectively. It is to be noted that no correlation between coupon weight loss and the hydrogen foil data was observed.

The trends in the variation of corrosion rates with the inhibitor concentration were used to compare the monitoring techniques.[52] For each inhibitor, the variation of corrosion rate with inhibitor concentration was determined at the top, middle, and bottom positions of the pipe. In order to compare the different corrosion monitoring techniques, a standard trend was developed. The standard trend was taken as 'the most repeated trend' (MRT) of different monitoring techniques. For example, the corrosion rates measured by one technique were: 50 at 0 ppm, 20 at 10 ppm, and 10 at 20 ppm. Then the trend in corrosion rates was 0, 10 and 20 ppm. This type of trend was deduced for each monitoring technique, and from this trend the MRT was deduced as the number of times the trend was repeated using different monitoring techniques.

Consider, for example, weight loss and linear polarization techniques. Let us assume these two techniques show a trend $0 > 50 > 100 > 200$ ppm, and the third technique (i.e.) hydrogen foils gives a trend $50 > 0 > 100 > 200$ ppm. The most repeated technique is in the order $0 > 50 > 100 > 200$. The trends

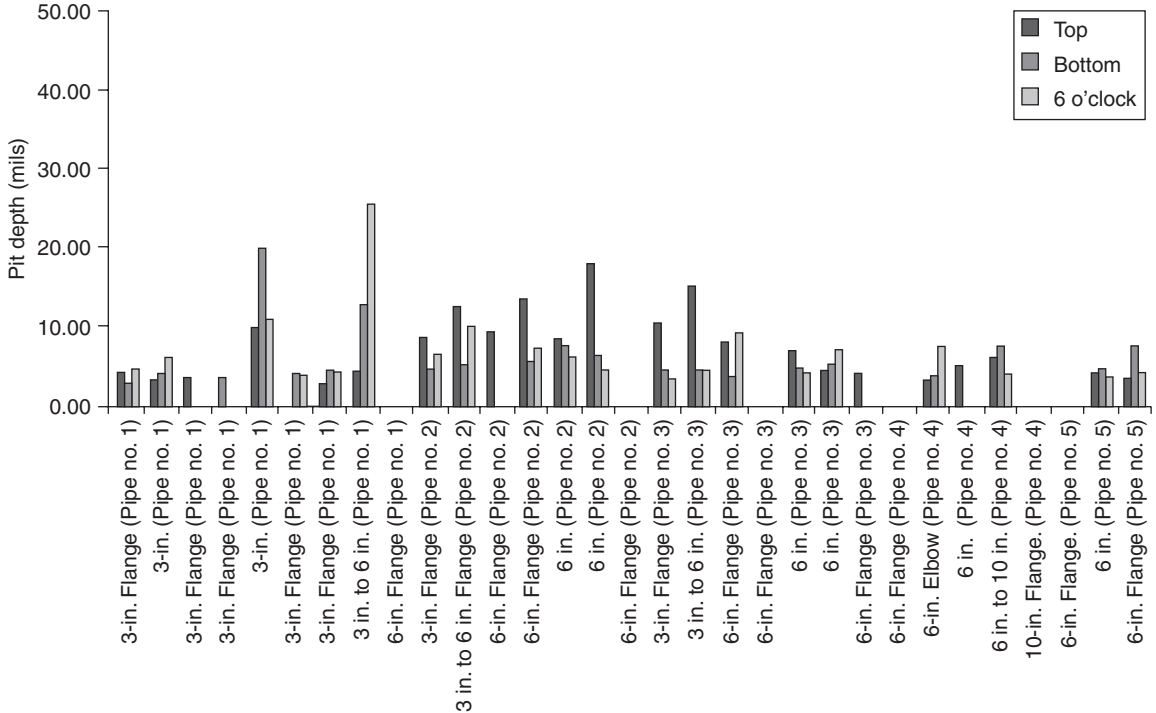

5.6 Pit depths in the inlet and outlet pipe sections (~ 2 years) exposed in all three fields (refer to Fig. 5.2 for different sections of the pipe. Pipe no. 1 = inhibitor injection port section; Pipe no. 2 = outlet section; Pipe no. 3 = inlet section; Pipe no. 4 = bend between replaceable and outlet sections; Pipe no. 5 = 90° bend between replaceable and inlet sections).

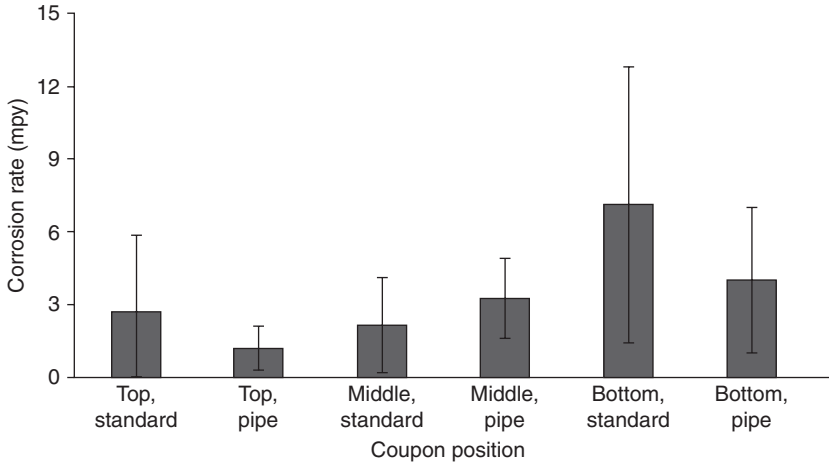

5.7 Comparison of general corrosion rate of standard and pipe coupons in gassy-oil field.

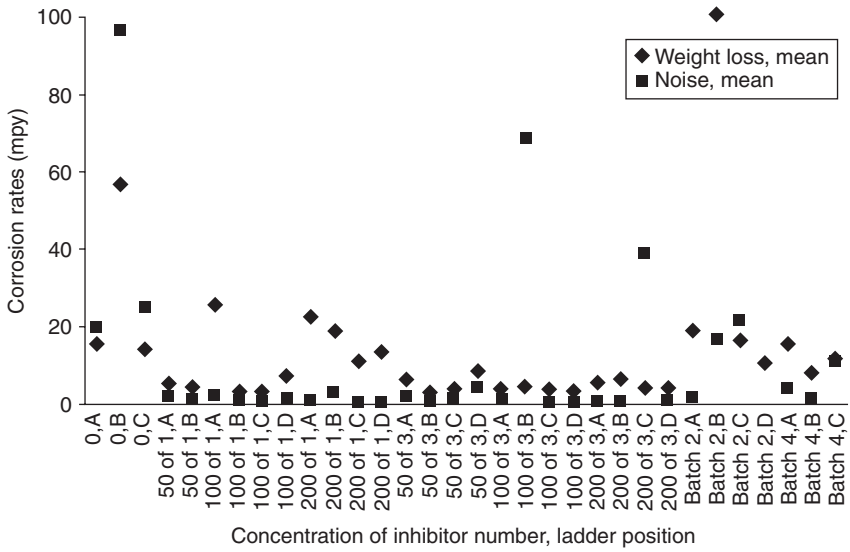

5.8 General corrosion rates of same coupon as measured by various techniques (gassy-oil field).

exhibited by the techniques were then compared with the mean repeated trend (MRT). In the above example, the weight loss data agree with MRT four times out of four comparisons (100%), while the hydrogen probe data agree two times out of four (50%). The technique with the closest agreement with MRT indicates most accurately the conditions in the pipe.

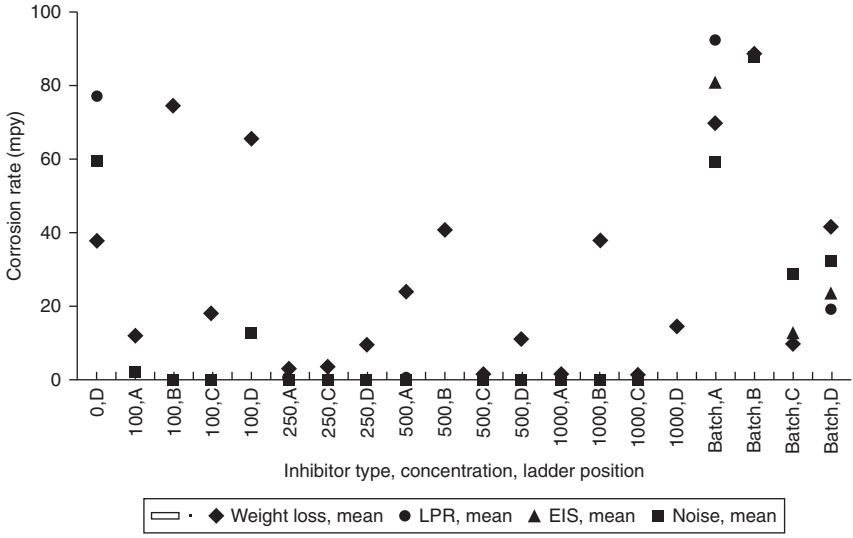

5.9 Corrosion rates of same coupon as measured by various techniques (oily-gas field).

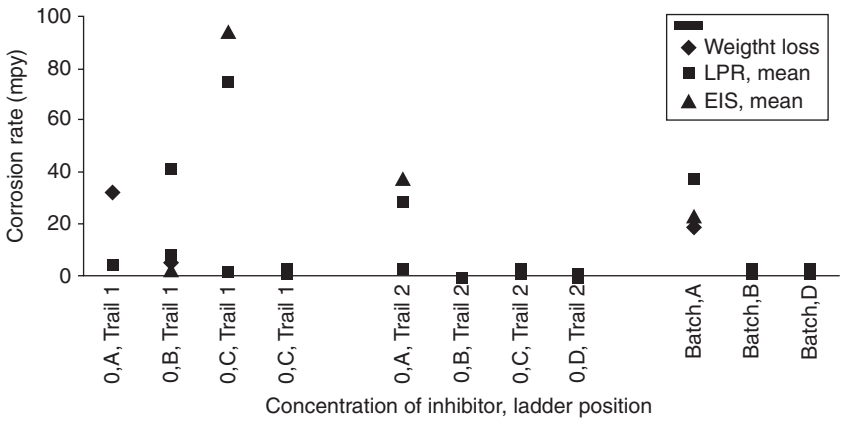

5.10 Corrosion rates of same coupon as measured by various techniques (oil-transmission field).

The MRT values obtained for general corrosion rates in gassy-oil, oily-gas and the oil-transmission field are presented in Tables 5.4–5.6 respectively. The rankings of the monitoring techniques are given in Table 5.7. For each monitoring technique, the percentage times the monitoring technique is in agreement with MRT values in each of three field conditions at the top, middle, and bottom positions were determined using the general corrosion rate

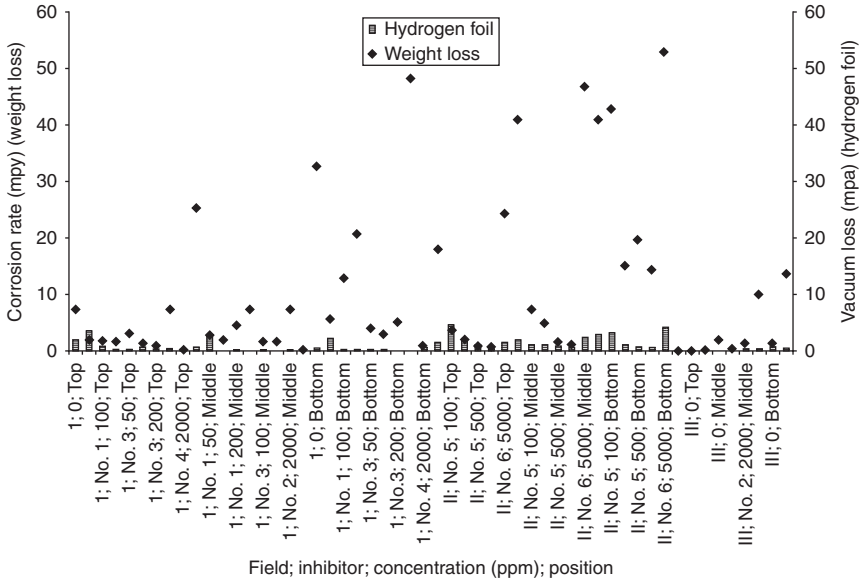

5.11 Comparison of general corrosion rates determined from weight loss and hydrogen permeation methods.

data. These calculations led to the final percentage agreement as follows: 91% EN, 89% weight loss, 70% LPR, 51% hydrogen sensors, and 33% EIS.

Pitting corrosion rates were obtained from the EN data in terms of pitting index, pitting factor, and pit indicator:

$$\text{Pitting index (PI)} = I_{\text{ms}} / I_{\text{mean}} \qquad [5.23]$$

where I_{rms} is the root mean square current noise, and I_{mean} is the mean coupling current. The PI values from 0–1 and PI value greater than 0.6 indicates localized corrosion:

$$\text{Pitting factor} = \frac{\left[\Delta i + \text{---} \Delta i\,(N)\right]}{n} \frac{\sigma_i}{I_{\text{rms}}} \qquad [5.24]$$

where Δi (1) is the current increase over a time interval, n is the number of readings taken during Δi, and σ_i is the standard deviation of current noise.

$$\text{Pit indicator} = \frac{\sigma_i}{I_{\text{mean}}} \qquad [5.25]$$

Table 5.4 Trends in the variation of general corrosion rates (gassy-oil) with inhibitor concentration

Technique	Variation of general corrosion rates (decreasing order)										
Top position											
Inhibitor	No. 1	No. 1	No. 1	No. 1	No. 3	No. 3	No. 3	No. 3	Batch	Batch	Batch
Weight loss	0	50	100	200	0	50	100	200	0	No. 2	No. 4
Pitting	0	50	100	200	0	50	100	200	No. 2	No.4	0
Hydrogen foil	50	0	100	200	0	100	200	50	0	No. 2	No. 4
MRT	0	50	100	200	0	50	100	200	0	No. 2	No. 4
Middle position											
Inhibitor	No. 1	No. 1	No. 1	No. 1	No. 3	No. 3	No. 3	No. 3	Batch	Batch	Batch
Weight loss	0	200	50	100	0	50	100	200	0	No. 2	No. 4
Pitting	0	50	100	200	0	50	100	200	No. 4	No. 2	0
Hydrogen foil	50	0	200	100	0	100	50	200	0	No. 4	No. 2
Noise	0	50	200	100	0	50	100	200	0	No. 2	No. 4
MRT	0	50	200	100	0	50	100	200	0	No. 2	No. 4
Bottom position											
Inhibitor	No. 1	No. 1	No. 1	No. 1	No. 3	No. 3	No. 3	No. 3	Batch	Batch	Batch
Weight loss	200	100	–	–	200	50	100	–	No. 2	No. 4	–
Pitting	100	200	–	–	50	100	200	–	No. 2	No. 4	–
Hydrogen foil	100	200	–	–	100	50	200	–	No. 4	No. 2	–
Noise	100	200	–	–	50	100	200	–	No. 4	No. 2	–
Noise, trap	200	100	–	–	100	50	200	–	No. 4	No. 2	–
MRT	100	200	–	–	50 and 100	50	200	–	No. 4	No. 2	–

Table 5.5 Trends in the variation of general corrosion rates (oily-gas) with inhibitor concentration

Measuring technique	Variation of general corrosion rates (decreasing order)						
Top position							
Inhibitor	No. 5	No. 5	No. 5	No. 5	No. 5	No. 6	No. 6
Weight loss	0	100	250	500	1000	5000	0
Pitting	0	100	250	500	1000	5000	0
Hydrogen foil	100	250	0	500	1000	5000	0
MRT	0	100	250	500	1000	5000	0
Middle position							
Inhibitor	No. 5	No. 5	No. 5	No. 5	No. 5	No. 6	No. 6
Weight loss	250	500	1000	–	–	–	–
Pitting	250	500	1000	–	–	–	–
Hydrogen foil	250	500	1000	–	–	–	–
Noise	250	1000	500	–	–	–	–
MRT	250	500	1000	–	–	–	–
Bottom position							
Weight loss	0	500	250	1000	–	5000	0
Pitting	0	1000	500	250	–	5000	0
Hydrogen foil	0	250	500	1000	–	5000	0
Noise	0	1000	500	250	–	5000	0
LPR	250	500	1000	0	–	5000	0
MRT	0	500 and 1000	500	250 and 1000	–	5000	0

Table 5.6 Trends in the variation of general corrosion rates (oil-transmission field) with inhibitor concentration

Measuring techniques	Variation of general corrosion rates (decreasing order)		
Top position			
Weight loss	2000	0, Trial no. 2	0, Trial no. 1
Pit rate	–	–	–
Hydrogen foil	2000	0, Trial no. 2	0, Trial no. 1
Middle position			
Weight loss	0, Trial no. 1	2000	0, Trial no. 2
Pit rate	0, Trial no. 1	2000	0, Trial no. 2
Hydrogen foil	2000	0, Trial no. 2	0, Trial no. 1
MRT	0, Trial no. 1	2000	0, Trial no. 2
Bottom position			
Weight loss	2000	0, Trial no. 1	0, Trial no. 2
Pit rate	2000	0, Trial no. 1	0, Trial no. 2
Hydrogen foil	0, Trial no. 2	0, Trial no. 1	2000
Noise	2000	0, Trial no. 1	0, Trial no. 2
LPR	2000	0, Trial no. 1	0, Trial no. 2
EIS	0, Trial no. 1	2000	0, Trial nno. 2
MRT	2000	0, Trial no. 1	0, Trial no. 2

Table 5.7 Agreement with most repeated trend

Position measuring techniques	Top			Middle			Bottom			Total			Final Rank
	No. of	No. of	% Agreement	No. of	No. of	% Agreement	No. of	No. of	% Agreement	No. of	No. of	% Agreement	%
Gassy-oil field													
Weight loss	11	11	100	11	9	82	7	1	14	29	21	72	–
Hydrogen foil	11	6	55	11	5	45	7	7	100	29	18	62	–
Noise	–	–	–	11	11	100	7	6	86	18	17	94	–
Oily-gas field													
Weight loss	7	7	–	3	3	100	6	5	83	16	15	94	–
Hydrogen foil	7	4	–	3	3	100	6	5	83	16	12	75	–
Noise	–	–	–	3	1	33	6	6	100	9	7	78	–
LPR	–	–	–	–	–	–	6	3	50	6	3	50	–
Oil-transmission field													
Weight loss	–	–	–	3	3	100	3	3	100	6	6	100	89
Hydrogen foil	–	–	–	3	0	0	3	1	33	6	1	17	51
Noise	–	–	–	–	–	–	3	3	100	3	3	100	91
LPR	–	–	–	–	–	–	3	3	100	3	3	100	91
EIS	–	–	–	–	–	–	3	1	33	3	1	33	33

The pits were measured using a micrometer on the electrochemically connected coupons and compared with the EN data such as pitting index, pitting factor, and pit indicator on the same sample coupon. While comparing pit measurements with EN pit parameters, it is necessary to note that noise measurements are instantaneous, and the pit depth measurements were done after the electrochemical experiment and pit depths on all the three electrodes, namely, working, reference and counter electrodes, are taken into account.

The pit depths measured on all three electrodes involved in the EN experiments and the noise pit parameters, namely pitting index, pitting factor, and pit indicator, were arranged in descending order. Pits were randomly initiated at various sites and different times, and for each pit formed on any one of the coupons (electrodes) there was a corresponding noise signal. The deeper the pit, the larger the noise signal. The noise signals were of high amplitude during the time the pits were growing. Each high amplitude signal was assumed to correspond to the growth of a single pit. The correlation factor, R^2, was determined from the plots of pit depths with each of the three noise pit parameters, as shown in Fig. 5.12. It is to be noted that the correlation between pit indicator and actual pits is better than the correlation with pitting index or pitting function.

The selection of corrosion inhibitors for oil and gas pipelines involves both laboratory testing and simulated field testing. The field testing involves dynamic conditions in the field and different types of monitoring methods, such as average, instantaneous, and continuous. The suitability of a monitored technique depends on the nature of the technique itself, as well as on the physical manner by which the monitoring technique can be used in the particular environment. The physical fit of the monitoring technique determines whether the data obtained are representative of the pipe or just the electrode/coupon/sensor. An experimental loop was used to evaluate both the behavior of the pipe and the coupon/electrode/sensor.

The laboratory flow loop testing done by various investigators, and the associated details, are summarized [53–65] in Table 5.8. The testing of a loop attached to an operating field pipeline was done and the pertinent details are given in Table 5.9. The field loop is a more realistic representation of the field conditions than the laboratory pipe loop.

It is useful to note that corrosion rate data obtained in the laboratory show some variability, but additional variability exists in field conditions due to the dynamic nature of the field conditions. Table 5.10 presents the fluctuations in the operating conditions of a gassy-oil field. The field experiments, in gassy-oil and oily-gas field for 15 days and for 30 days in transmission-oil fields, were done to counter the variability of the field conditions.

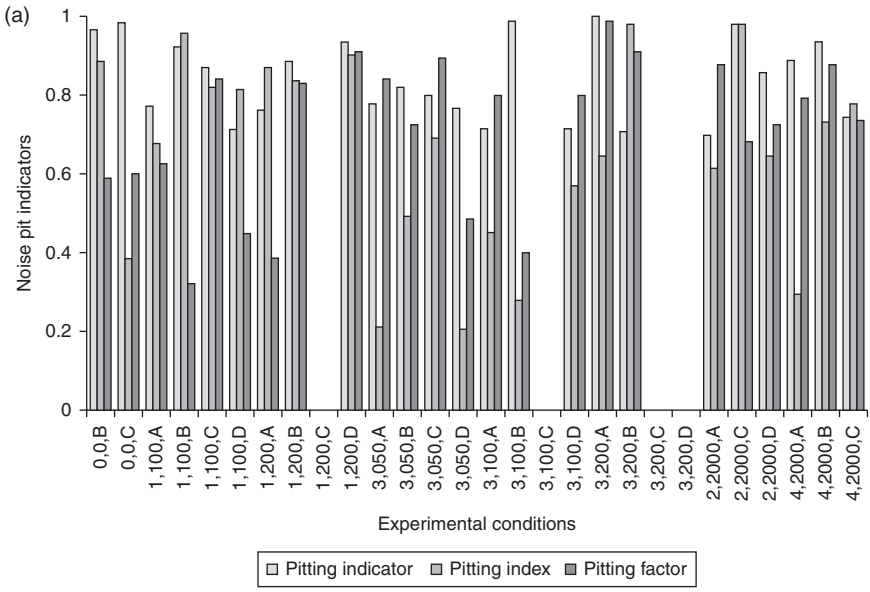

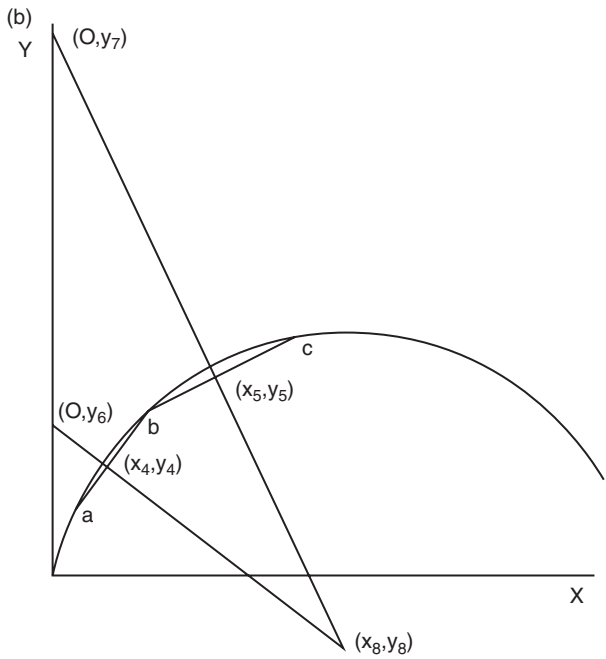

5.12 (a) *R*2 values for the correlation between measured pits vs pitting corrosion as indicated by noise measurements. (b) Three-point geometric technique representation.

Table 5.8 Characteristics of laboratory pipe loop

		Pipe dimension			Maximum[a]			
Material	Measuring techniques	Diameter of experimental section (cm)	Capacity (L)	Probes/ coupons	Flow rate (m/s)	Temperature. (°C (°F))	Pressure psi (kPa)	Reference
Nickel alloy C-276	LPR and EIS	1.5 (ID)	75	Flat and flush-mounted tubular	10	150 (270)	725 (5000)	54
Type 316 SS	EIS	10 (OD)	141	Flush-mounted	1	90 (162)	300 (2068)	55
Acrylic	EIS and electrical resistance (ER) probes	10 (ID)	141	Flush-mounted	6,9,12[b]	40 (104)	20 (138)	56
Alloy C	LPR and weight loss	1.59 (ID)	1.5	Tubular	50, 150, 990[c]	65 (150)	40 (275)	57
Type 316L SS (UNS S31600); nickel alloy C-276 (UNS N10276); and titanium (UNS R50250)	Weight loss	1.27 (OD)	–5	Annular tube	15.2	149 (300)	600 (4137)	58
SS	Weight loss	Volume/coupon ratio 161 or 2 L/cm^2		Annular tube	9	77 (170)	160 (1103)	59
Alloy C-276	LPR and weight loss	1.27	5	Tubular samples	11	93 (200)	150 (1000)	60
Type 316 SS	Weight loss and EIS	2.54 (ID)	3.78	Annular	1.8	93 (199)	595 (4100)	61

(*Continued*)

Table 5.8 Continued

		Pipe dimension			Maximum[a]			
Material	Measuring techniques	Diameter of experimental section (cm)	Capacity (L)	Probes/ coupons	Flow rate (m/s)	Temperature. (°C (°F))	Pressure psi (kPa)	Reference
Type 316 SS	Weight loss	6.5(ID)		Intrusive coupons and flush-mounted samples	5	180 (356)	870 (6000)	62
	LPR and EIS	1.27 and 2.54 (ID)		Flush-mounted ring electrodes	2–300[c]	50 (122)	Atmospheric	63
C steel (N80) or 13Cr martensitic SS (UNSS42000)	Weight loss and LPR	1.0 (ID)	0.009	Cylindrical specimen	20 (liquid) 100 (gas)	300 (572)	1450 (10 000)	64
Type 316 SS	EIS	0.9 (ID)		Flush-mounted	7	75 (135)	81 (560)	65
C-276 SS	Weight loss and electrochemical	0.6 (OD)	6	Cylindrical specimen	3	38 (100)	1000 (6895)	66

[a]Maximum values for the system or values at which the results are presented.
[b]Froude number.
[c]Wall shear stress.

Table 5.9 Comparison of laboratory and field flow loops used in the present study

Laboratory flow loop	Field flow loop (used in the present study).
Conditions controlled by the performer	Conditions set by the field operation
Usually made of corrosion-resistant materials	Made of carbon steel
Comparison between coupons/probes/electrodes in the loop and the loop itself cannot be made	A quantitative comparison between coupons and the pipe can be made, because some coupons are made out of the pipe material
Reusable (after proper cleaning)	The loop was completely destructed to determine the pit distribution on the inside wall
Fluids can be recirculated. Care should be taken to avoid saturation of solution with corrosion products	Once-through only
Electrodes/probes can be placed as a part of the loop body (with proper spacer for electrode insulation)	Safety regulation of an operating pipeline does not permit reliable placement of electrodes/probes as part of pipe body

Table 5.10 Fluctuations in the operating conditions of gassy-oil field

Experimental conditions		Production (m^3/D)			Pressure (kPa)	Temperature (°C)
Inhibitor	Concentration	Water	Oil	Gas × 10^3		
Uninhibited	0	181	66	20	2600	56
Batch no. 2	2000	160	49	18	1800	57
Batch no. 4	2000	168	51	18	1700	57
Inhibitor no. 1	50	138	37	11	2300	54
Inhibitor no. 1	100	160	42	19	2100	54
Inhibitor no. 1	200	203	43	13	1700	56
Inhibitor no. 3	50	178	42	16	1700	56
Inhibitor no. 3	100	167	49	16	1500	57
Inhibitor no.3	200	163	48	18	1600	57

There have also been studies on the effect of flow rates on corrosion. The effect of flow rate on the corrosion rate in inhibited 15% HCl showed acceleration of corrosion rate with increasing flow velocity between 65°C and 70°C. The effect of flow rate on the inhibitors tested at 125°C was negligible.[66] The methods used for the evaluation of inhibitors and changes in the metal surface induced by acid stimulation treatment consisted of reflectance Fourier transform infrared spectroscopy,[67] nuclear magnetic resonance (NMR) and size exclusion chromatography, contact angle measurement,[68] linear polarization,[69] and conventional techniques such as potentiostatic polarization,

cyclic voltammetry, and determination of concentration of iron in solutions as a function of time.

5.5 The use of coupons to measure corrosion rates

Sample coupons can be placed, removed, and replaced periodically to provide continuous data on the relative corrosivity and the inhibitor efficiency. Placement and retrieval of coupons are straightforward, and can be done under pressure without stopping production. The sample coupons are flush-mounted or placed as part of the pipe for proper pipe–coupon correlation. This type of placing sample coupons is not impossible but can be done in the operating pipe only by shutting down operations. Sample misalignment can lead to large errors in corrosion rates.[70]

The coupon and pipe behavior should be correlated to obtain meaningful results. Such correlations can be made only when the geometry and types of coupons are protruding or flush, the chemical composition of the pipe and coupons is the same, the corrosion mechanisms of coupon/electrode and the pipe are the same and the electric isolation of coupon/electrode from the pipe exists. Improper positioning of sample coupons is subject to erosion from the edges. In the cases of coupons/electrodes protruding in nature are subject to exposure to severe flow conditions unlike the pipe and represents a worst-case corrosivity of the pipe.

Protruding coupons/electrodes in general showed higher pitting rates than the pipe itself. Slight differences in the metallurgy of the sample coupons and surface finish (polishing) had very little effect on the corrosion behavior as seen in Fig. 5.7. Sample coupons placed in the top portion of the pipe exposed to gas-oil phases were subject to less corrosion. Sample coupons placed in the middle of the pipe were exposed to oil and water phases and subject to moderate to severe corrosion. The samples in the bottom of the pipe were exposed fully to corrosive brine and corroded and pitted to a greater degree. The sample coupons at the bottom of the pipe represent the worst-case corrosive scenario of the pipeline.

5.6 Comparing different monitoring techniques

Corrosion rates obtained by various techniques in oil and gas pipelines can be compared as follows. The weight loss technique proved to be the most reliable technique for monitoring corrosion inhibition of general and pitting corrosion rates. The weight loss data agreed about 90% MRT. Since the method is time-averaged, some prior knowledge or judgment is required with respect to the duration of sample coupon exposure.

The LPR general corrosion rate agreed nearly 70% of the time with MRT (Table 5.8). In many practical situations, the Tafel slopes were taken

as $\beta_a = \beta_c = 60$ V or 100 V/decade. The calculated corrosion rates from electrochemical data with assumed Tafel slope values have been found to be correct within a factor of 2.2. This is a non-destructive, straightforward, simple technique that can be used for long-term monitoring in oil and gas pipelines. This technique gives instantaneous general corrosion rates, so that the effect of inhibitors and the variation in inhibitor concentration can be determined. The technique does not give any information on localized corrosion.

General corrosion trends obtained by EIS agreed with MRT about 33% of the time. Collection of data by EIS over a wide frequency range requires a long time. Fast Fourier transform (FFT) reduces the time duration of collection of data to a considerable extent. For instance, the FFT technique can be used to obtain data at 20 frequencies between 0.001 Hz and 0.1 Hz in 1000 s, as opposed to data at one frequency in 1000 s by conventional methods. This technique requires a physical model to analyze the data. The technique also requires an equivalent circuit representing the corroding metal coated with a porous non-conducting film.

A geometric technique, in which the centers formed by three successive data points at three frequencies are determined, was used for analyzing the AC impedance diagrams (Fig. 5.12) obtained experimentally.[71] The equivalent electrical circuit that represents a simple electrochemical reaction, along with the impedance diagram, is shown in Fig. 5.13. The charge transfer resistance (polarization resistance) R_p can be evaluated from the diameter of the semicircular impedance diagrams. Corrosion rates are then related to

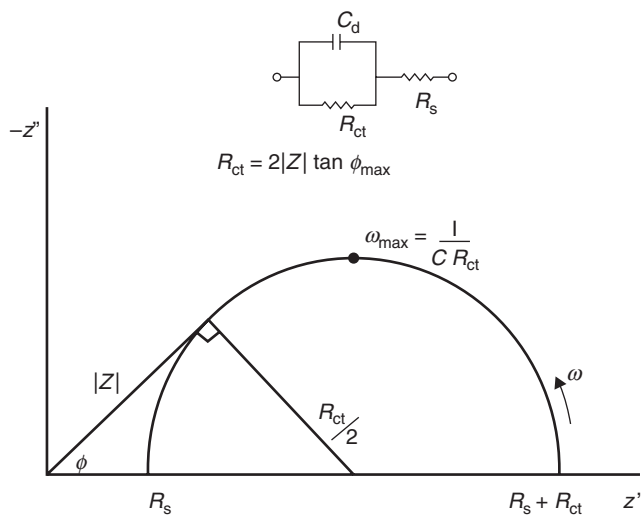

5.13 Representation of equivalent circuit.

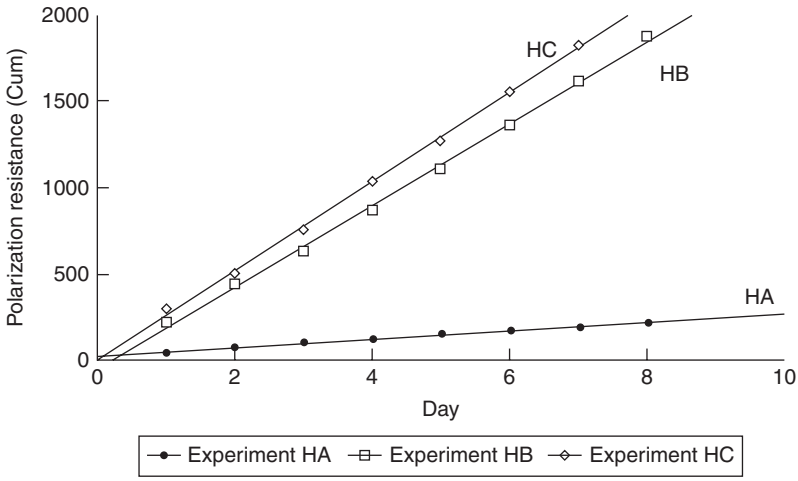

5.14 Cumulative polarization resistance vs time.

R_p, the polarization resistance ($1/R_p$) by the Stern-Geary low overvoltage approximation of the Butler-Volmer equation.

The data on polarization resistance for process water devoid of any inhibitor, and process water containing inhibitors HB and HC, are shown in Fig. 5.14. The cumulative polarization resistance for solutions with inhibitors increases rapidly, while the value stays the same for process water devoid of inhibitor. The sum of depression angles is shown in Fig. 5.15 for the two inhibitors as a function of time. The sum of depression angle shows a steep increase in process water devoid of inhibitor, and a very small increase in depression angle in solutions with inhibitors (HB and HC). The depression angle is indicative of localized corrosion. Thus AC impedance is capable of monitoring corrosion in the field as well as in the laboratory by obtaining the R_p values at three frequencies.

The general corrosion rate trend obtained by the EN technique agreed to 90% of MRT. When a sample coupon is exposed to corrosive fluids, several events such as general corrosion, erosion corrosion due to flowing fluids, passive film formation and breakdown, pit initiation, and repassivation occur. Each event generates an electrochemical current, the magnitude and sign of which depend on the nature of the event. All the EN fluctuations are measured. During pit growth, a higher magnitude current signal is observed. This signal is manifested as the standard deviation the magnitude of which is greater than the mean current value. The ratio of standard deviation to the mean current indicates pit growth, known as the pit indicator equation, σ_i/I_{mean}. The EN method has been found to be a promising method for monitoring corrosion in oil pipelines. A typical electrochemical cell, and the

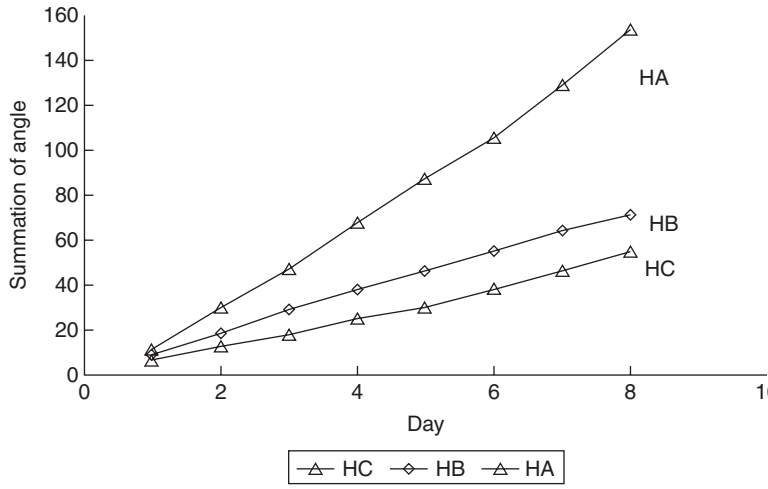

5.15 Summation of angle vs time.

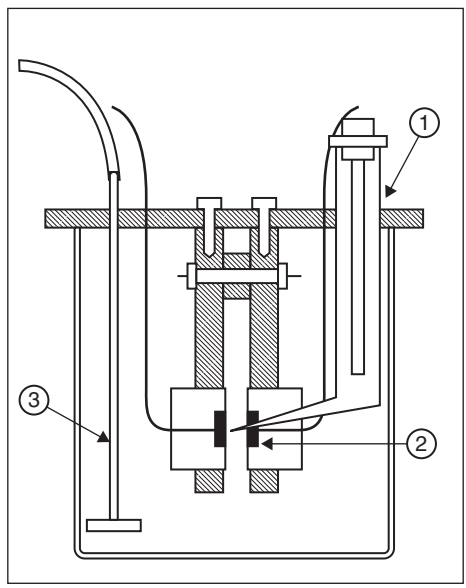

1) Calomel reference electrode
2) Steel specimen
3) Gas purge

5.16 Electrochemical cell.

experimental arrangement of the apparatus used in potential noise measurements, are shown in Figs 5.16 and 5.17 respectively. Figure 5.18a shows the electrochemical potential noise response in process water with and without added inhibitor as a function of time.

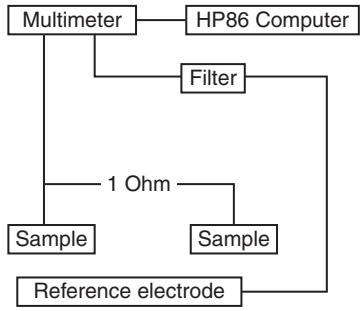

5.17 Apparatus used for potential noise measurements.

The results obtained from the hydrogen permeation technique did not correlate with the data obtained from intrusive techniques. The hydrogen permeation method of monitoring internal corrosion rates is nonintrusive. Some of the factors that influenced hydrogen permeation measurements are gluing of foil, length of the capillary tube, temperature fluctuations, pipe wall thickness, and the fraction of hydrogen atoms produced by the corrosion reaction that enter the foil. This technique may be used in pipelines where corrosion occurs in small areas in which water accumulates, but is not recommended in pipelines in which corrosion occurs over larger surface areas.

5.7 Conclusion

A survey of monitoring techniques based on categories listed in NACE 3T 199, such as direct intrusive physical techniques, direct intrusive electrochemical techniques, direct nonintrusive measurement techniques, indirect online measurement techniques, indirect offline measurement techniques, and MIC measurement technique resulted in the data illustrated in Fig. 5.18b, 5.18c, 5.18d, 5.18e, 5.18f, and 5.18g.

The techniques for monitoring internal corrosion in pipelines can be broadly classified into direct intrusive physical techniques, direct intrusive electrochemical techniques, direct nonintrusive techniques, indirect online monitoring techniques, indirect offline monitoring techniques, MIC monitoring techniques, and new techniques.

The more reliable the technique, the greater its usage, but no single technique is outstanding and unique in meeting all the requirements of corrosion monitoring. The factors that influence decisions for selecting an appropriate monitoring technique are the reliability of the technique and its tolerance to the variable operating conditions.

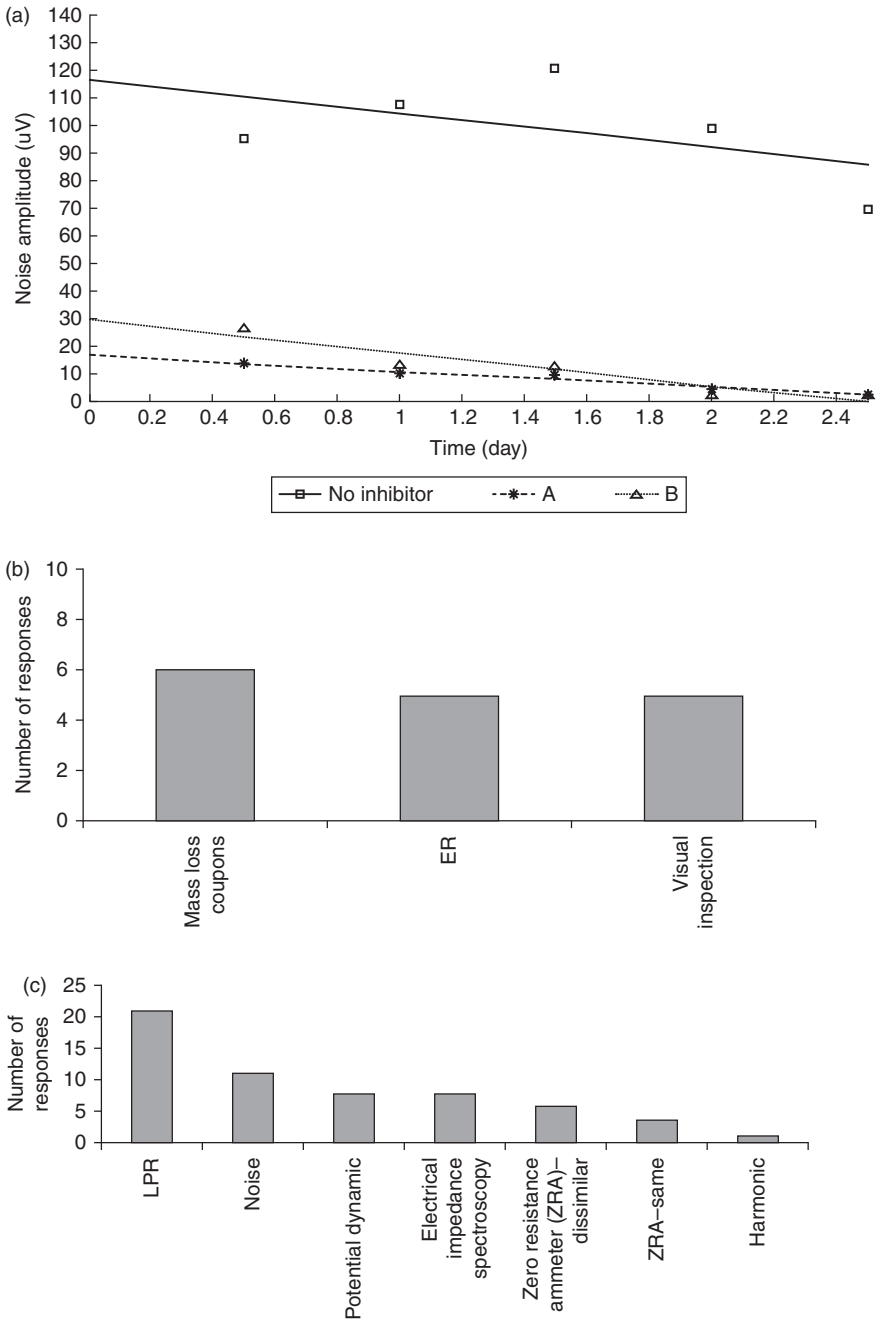

5.18 (a) Potential noise amplitude vs time. (b) Direct intrusive physical techniques. (c) Direct intrusive electrochemical techniques. (d) Direct nonintrusive measurement techniques. (e) Indirect online measurement techniques. (f) Indirect offline measurement techniques. (g) MIC measurement techniques.

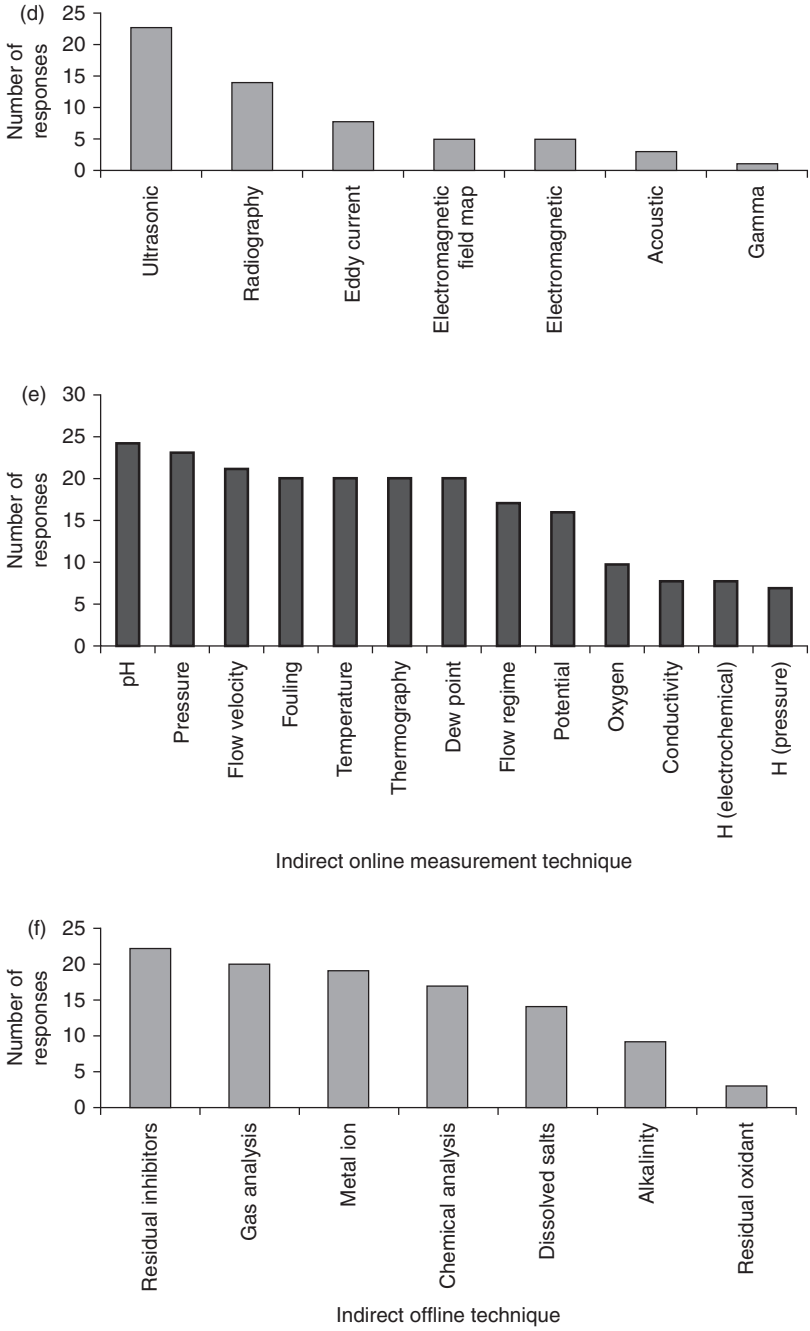

5.18 Continued

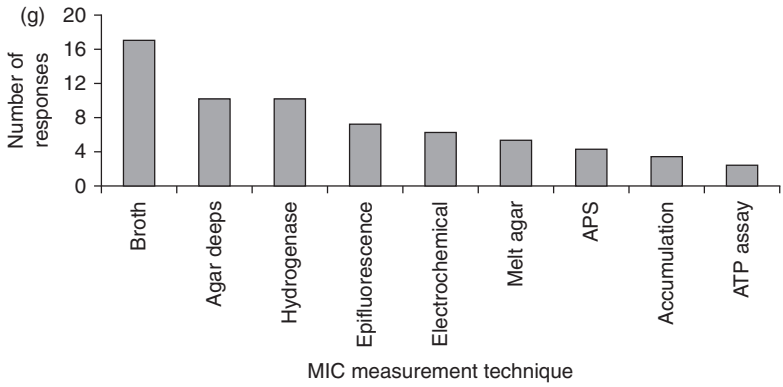

5.18 Continued

It is useful to note that the survey were not analyzed based on the technical background of the respondents, nor was the ratio of people in different categories established. Therefore, the error due to person bias of respondents was included in the results. Thus, the results of the survey of monitoring techniques should be considered more as a trend at the time the survey was commissioned.

5.8 References

1. Nestle A (1973), *Corrosion Inhibitors in Petroleum Production Primary Recovery*, Houston, NACE.
2. Tuttle R N and Kane R D (1973), *H_2S Corrosion in Oil and Gas Production: Classic Paper*, Houston, NACE.
3. Bregman J I (1966), 'Proc. 2nd SEIC', *Ann Univ Ferrara*, n.s., Sez V., suppl. no. 4, 549.
4. Bregman J I (1971), 'Proc. 3rd SEIC', *Ann Univ Ferrara*, n.s., Sez. V, suppl. no. 5, 339.
5. Foroulis Z A (1980), 'Proc. 5th SEIC', *Ann Univ Ferrera*, Sez. V, suppl. no. 7, 1029.
6. Lahodny-Sarc O (1985), 'Proc. 6th SEIC', *Ann Univ Ferrara*, Sez V, suppl. no. 8, 1313.
7. Hausler R H and Stegmann D W (1990), 'Proc. 7th SEIC', *Ann Univ Ferrara*, n.s., Sez. V, suppl. no. 5, 427.
8. Reiser K (1966), 'Proc. 2nd SEIC', *Ann Univ Ferrara*, n.s., Sez. V, suppl. no. 4, 459.
9. Balezin S A and Kemhadze T V (1971), 'Proc. 3rd SEIC', *Ann Univ Ferrara*, n.s., Sez. V, suppl. no. 5, 427.
10. Schmitt G and Bruckoff W (1980), 'Proc. 5th SEIC', *Ann Univ Ferrara*, n.s., Sez. V, suppl. no. 7, 323.